Zhao *et al. Journal of Wood Science* (2022) 68:62
https://doi.org/10.1186/s10086-022-02070-1

Journal of Wood Science

ORIGINAL ARTICLE

Open Access

Influence of boundary conditions on acoustic emission propagation characteristics of *Zelkova schneideriana*

Yue Zhao[1], Ming Li[2,3*], Saiyin Fang[1], Shaochun Zhang[1], Changlin Huang[1], Tingting Deng[1], Feilong Mao[1], Gezhou Qin[1] and Daigen Zhu[1]

Abstract

To study the propagation characteristics of acoustic emission signals in *Zelkova schneideriana* under different boundary conditions, three types of boundary conditions were generated by applying aluminum plates and sound-absorbing cotton on the surface of *Zelkova schneideriana* specimens. Firstly, the sudden and continuous acoustic emission (AE) sources were simulated by PLB (pencil–lead break) tests and signal generator on the specimen surface, and the AE signals were collected by 5 sensors equally spaced on the surface of the specimen, and the sampling frequency was set to 500 kHz. Then, the detailed signals of different frequency bands were obtained by wavelet decomposition, and TDOA (the time difference of arrival) and correlation analysis method were used to calculate the time difference of longitudinal wave and surface transverse wave and the corresponding propagation velocity, respectively. Finally, the pulse trains with different energy levels generated by the signal generator were used as AE sources to study the attenuation law of AE signal energy with distance under different boundary conditions. The results show that the boundary changes can lead to a significant increase in the surface transverse wave velocity, and have no significant effect on the longitudinal wave velocity. At the same time, the energy attenuation of surface and longitudinal waves is faster after the aluminum plate and sound-absorbing cotton are affixed, and the distance of longitudinal waves attenuation to 90% is reduced from 186 to 139 mm, and the distance of surface transverse waves propagation is reduced from 312 to 226 mm.

Keywords: Wood, Acoustic emission, Boundary conditions, Wavelet transform, Attenuation rate

Introduction

Acoustic emission (AE) refers to the phenomenon that the strain energy is released in the form of transient elastic wave when the material is deformed and fractured by external force or internal force [1]. AE technology as a non-destructive testing method, has been widely used in metals, wood, and composites [2–4].

AE technology is widely used in wood processing monitoring, drying and fracture damage. For example, Kawamoto et al. used AE to monitor defects during wood drying [5]. Kim et al. used principal component analysis and artificial neural network to classify AE signals in oak drying process, and the results showed that AE technology could effectively monitor the drying process of wood [6]. In recent years, AE has also been applied to wood processing monitoring. Vahid et al. effectively monitored the sawing process of fir under extreme cutting conditions by extracting AE signal characteristics [7]. Bucur et al. used AE technology to study the relationship between wood internal crack propagation and AE signal characteristics [8]. Lamy et al. [9] used AE technology to

*Correspondence: 1841719811@qq.com

[2] Key Laboratory of Advanced Perception and Intelligent Control of High-End Equipment of Ministry of Education, Anhui Polytechnic University, Wuhu 241000, Anhui, China
Full list of author information is available at the end of the article

study the failure process of wood under monotonic loading [9]. Li et al. studied the acoustic emission signal propagation characteristics of *Pinus massoniana* plywood using AE technology [10]. In the current study, most researchers have used pencil–lead break (PLB) as the AE source to simulate the damage of materials and to clarify the propagation characteristics of the AE signal generated by the simulated damage source [11–15]. Wang et al. verified that PLB tests can effectively simulate wood damage. At the same time, the effect of surface cracks on AE signals was studied by PLB tests. The results showed that surface cracks had an effect on the spectrum characteristics and propagation speed of AE signals [16, 17]. Shen et al. [18] used the method of spectral analysis to study the AE signals in the process of wood damage and fracture. The results showed that it can be divided into three categories according to the characteristic spectral analysis of AE signals in the process of wood damage and fracture. The propagation of acoustic emission in a structure was accompanied by reflection, attenuation and phenomena [19]. To study the energy attenuation law of different waveforms in wood, Zhao et al. established an energy attenuation model to study the location of the damage source of wood tenon structure by simulating the acoustic emission source through PLB tests. The location of the damage source of wood tenon structure was determined using the energy attenuation model and the method of two-point localization method, and the results of the study showed that the energy attenuation model was applicable to wood [20]. Li et al. [21] and Ding et al. [22] studied the energy attenuation law of surface shear wave and internal longitudinal wave in wood by designing the separation test of surface shear wave and internal longitudinal wave. The results showed that the energy of surface shear wave and internal longitudinal wave decreased exponentially. There are two methods for processing and analyzing AE signals: one is parametric analysis and the other is wavelet analysis [23, 24]. Li et al. [25] used wavelet analysis method to study the AE signal characteristics of *Pseudotsuga menziesii* plywood beam, and calculated the propagation velocity of AE signal in the surface direction of *Pseudotsuga menziesii* plywood beam. Liu et al. [26] carried on the noise reduction processing to the particleboard compression acoustic emission signal through the wavelet analysis method, the results showed that the wavelet analysis can well retain the mutation part of the AE signal, which can effectively reduce the influence of noise. Li et al. [27] used wavelet analysis to extract AE signals in different frequency bands on the surface and inside of camphor pine, and used the AE signals with the effective frequency band to calculate the propagation velocity, and the research results showed that the accuracy of calculating the propagation velocity of AE signals could be effectively improved. The propagation speed of AE signal is calculated according to the propagation time difference between the two sensors and the distance between the sensors, the commonly used method to calculate the propagation time difference is signal correlation analysis [28–30].

At present, most studies on the AE characteristics of wood only focus on the AE signals of wood cracks and wood surface. However, in practical engineering applications, wood is often closely connected with other types of materials. To study the influence of different boundary conditions on the propagation characteristics of AE signals in wood, this paper takes *Zelkova schneideriana* as the experimental material, selects isotropic metal aluminum plate and anisotropic porous media material sound-absorbing cotton, and closely adheres them to the wood surface. The original boundary conditions of wood are changed. Lead core fracture and signal generator are used as simulated AE sources, and on the basis of lead core fracture. The propagation velocity of AE longitudinal wave and surface wave is calculated by the time difference of arrival (TDOA) and correlation analysis. Finally, the 150 kHz pulse signals with different voltage levels generated by the signal generator are used as AE sources to study the influence of boundary conditions on AE energy attenuation.

Materials and methods

Experimental materials

The *Zelkova schneideriana* specimen with smooth surface and no defect was selected, and its size was 800 mm × 60 mm × 30 mm, the density was 0.72 g/cm^3, moisture content (MC) was 11.8%. The test specimens were divided into four groups, the boundary conditions of 3 groups were changed, and the specimens without boundary conditions were recorded as T1, while the specimens with aluminum plate, sound-absorbing cotton, aluminum plate and sound-absorbing cotton on the wood surface were recorded as T2, T3and T4, respectively, as shown in Fig. 1. The 5-channel AE signal acquisition system was built by NI USB-6366 high-speed acquisition card and Lab VIEW 2017 software (National Instruments of America). The RS-2A single-end resonant AE sensor was selected, whose bandwidth is 50 to 400 kHz. To realize the long-distance transmission of AE signals, the PAI front-end amplifier with gain of 40 dB was used, as shown in Fig. 2. During the test, the sampling frequency of the system was set to 500 kHz, and the output range of the output voltage was set to (− 5 V, 5 V). The signal generator model was SIGLENT-SDG805, the sampling channel is single channel, the maximum output frequency is 5 MHz, the maximum sampling rate is 125 MSa/s, and the output voltage range is 4 mVpp to 20 Vpp.

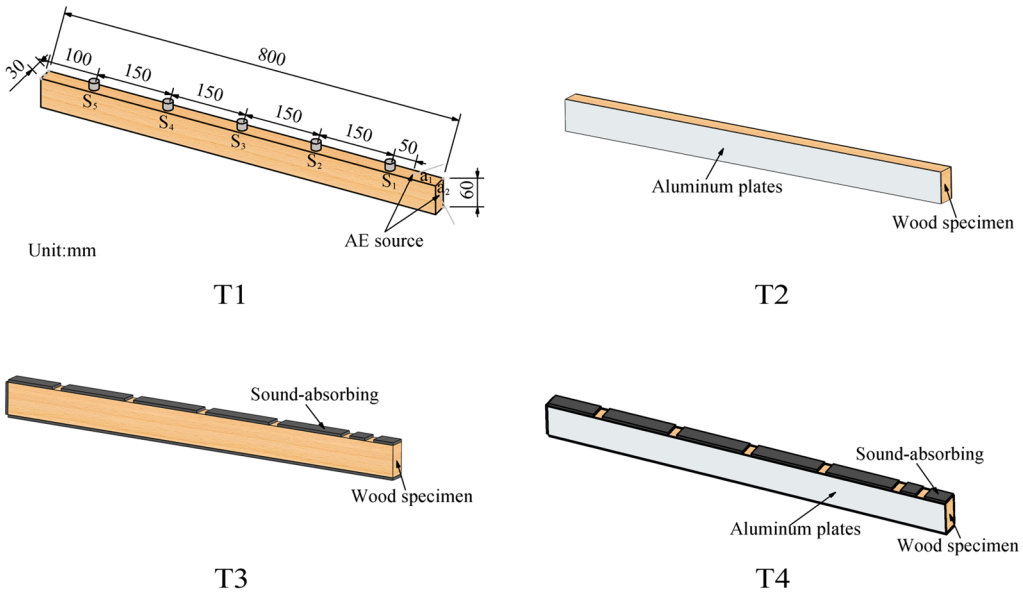

Fig. 1 Classification of specimens

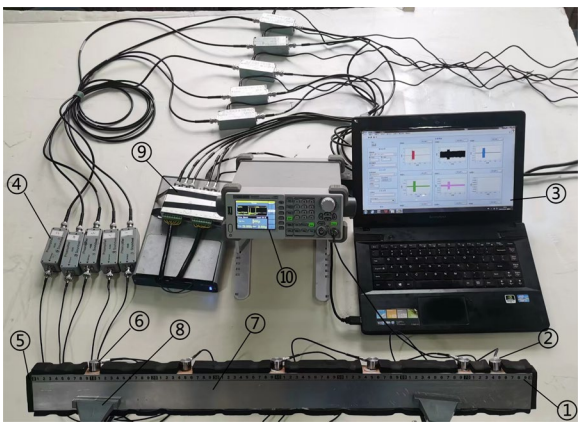

Fig. 2 Schematic diagram of the test scheme. ① Ruler ②AE source ③AE signal acquisition computer ④PAI front-end amplifier ⑤Sound-absorbing cotton ⑥Sensors ⑦Aluminum plate ⑧Vise ⑨NI acquisition card ⑩Arbitrary waveform generator

Experimental method

According to of the United States [31], the automatic pencil lead with a diameter of 0.5 mm was placed at an angle of 30° with the specimen surface, and the sudden AE source was broken at 2.5 mm away from the contact point to calculate the propagation velocity of AE signal in wood. A signal generator was used to generate a 150 kHz burst to analyze the energy attenuation of the AE signal in the wood. As shown in Fig. 1, the acquisition sensor was placed at an equal distance of 150 mm in the experiment, and the distance between the sensors on both sides of the sensor and the left and right end faces was 100 mm, which was S_1 to S_5 from right to left. According to the mechanical wave vibration theory, the particle vibration direction of shear wave is perpendicular to the propagation direction of wave, and the particle vibration direction of longitudinal wave is parallel to the propagation direction of wave. Therefore, when the burst and continuous AE sources are generated at the a_1 position of the wood surface, the signal detected by the sensor S_1 to S_5 is mainly the shear wave of the wood surface [21], and when the burst and continuous AE sources are generated at the a_2 position of the wood end face, the signal detected by the sensor S_1 to S_5 is mainly the longitudinal wave of the wood.

The frequency components of AE signals produced by PLB are complex and the distribution frequency domain is wide, to extract clearer AE signals, wavelet analysis is used to decompose them into four layers. According to the multi-resolution analysis theory of the wavelet transform, the frequency ranges of the four-layer detail signals decomposed by wavelet are (125 kHz, 250 kHz), (62.5 kHz, 125 kHz), (31.25 kHz, 62.5 kHz), (15.625 kHz, 31.25 kHz).

To study the propagation velocity of AE surface transverse wave and longitudinal wave in wood, the propagation time difference Δt was determined by TDOA. On the basis of wavelet analysis, the propagation velocity of AE surface wave was calculated by signal correlation. According to the elastic wave theory, the propagation velocity of the longitudinal wave in the material is greater than that of the surface transverse

wave. The first wave received by the sensor is mainly composed of the longitudinal wave, and the longitudinal wave velocity is calculated by TDOA. The distance Δs of the sensors remains unchanged during the test, and the propagation speed of AE signal can be calculated according to $v = \Delta s/\Delta t$. Cross correlation function represents the similarity between two signals, the cross correlation function of signals $x(t)$ and $y(t)$ is defined as

$$R_{xy}(\tau) = \lim_{T\to\infty} \frac{1}{T}\int_0^T x(t)y(t+\tau)d_t \quad (1)$$

When $\tau = \tau_0$, the absolute value of the cross-correlation function $|R_{xy}(\tau_0)|$ reaches the maximum, and it means that the signal $y(t)$ has the highest similarity with the signal $x(t)$ after τ_0 units are shifted on the time axis. To calculate the energy of the AE signal of the specimen, the AE signal is regarded as the alternating current. The energy of the AE signal is the heat generated by the AE signal through the unit resistance in a certain time:

$$W = \int_0^t \frac{U^2}{R} d\tau \quad (2)$$

The AE signal collected through the system is discontinuous, Eq. (2) needs to be discretized, and the two data are separated by $1/f_s$ second. Assuming that the discrete process adopts zero-order retainer, that is, the amplitude of the signal remains unchanged during this period, then the AE signal energy can be calculated as Eq. (3):

$$W = \sum_{i=1}^n \Delta t_i \cdot u_i^2 = T\sum_{i=1}^n u_i^2 \quad (3)$$

$\Delta t_i = T = 1/f_s (i = 1, 2, \ldots, n)$, where f_s is the sampling frequency and n is the data length.

Results and discussion

Surface transverse wave velocity of AE signal under different boundary conditions

Teodorovich et al., Pang et al. and Calvet et al. extracted and analyzed the features of the fading signal using AE signal features, spectrum and pattern recognition [32–34].

Figure 3 shows the time-domain signal and standing wave spectrum generated by the PLB, from top to bottom are sensors S_1 to S_5, respectively. As shown in Fig. 3a, all five sensors have a relatively stable wave in the time domain signal, which is considered as a "standing wave". According to the theory of elastic wave, standing wave refers to two kinds of waves with the same frequency and opposite transmission direction. One wave is generally the reflected wave of another wave, and the standing wave always exists in the propagation process of AE signal. To clarify the frequency domain characteristics of the standing wave, the stable waves corresponding to the five sensors are intercepted and analyzed by fast Fourier transform. As shown in Fig. 3b, the principal components of the five sensors are concentrated around 5 kHz. When calculating the surface wave velocity, to eliminate the influence of standing wave, wavelet analysis was used to denoise the AE signal.

Figure 4 shows the wavelet analysis layering diagram, based on wavelet theory, the AE signal is decomposed by 4 layers of wavelets to remove the standing wave components in the frequency band centered at 5.9 kHz. AE signals collected by sensor are mainly distributed in d1 and d3 frequency bands, and the proportion of d2 and d4 components in the signal is small. d1 is mainly dominated by high frequency, because the porous structure

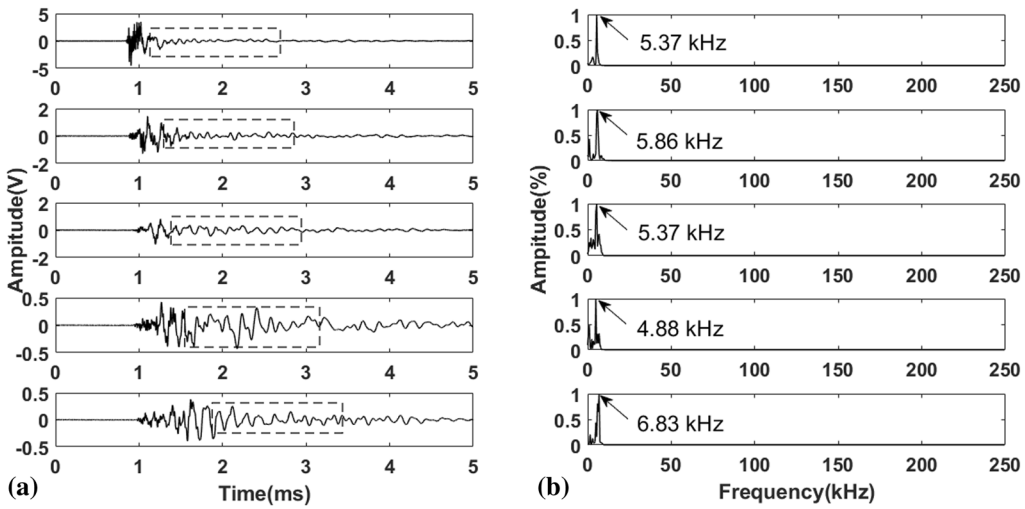

Fig. 3 AE waveform and standing wave frequency domain of PLB. **a** AE waveform produced by lead breaking. **b** Standing wave spectrum

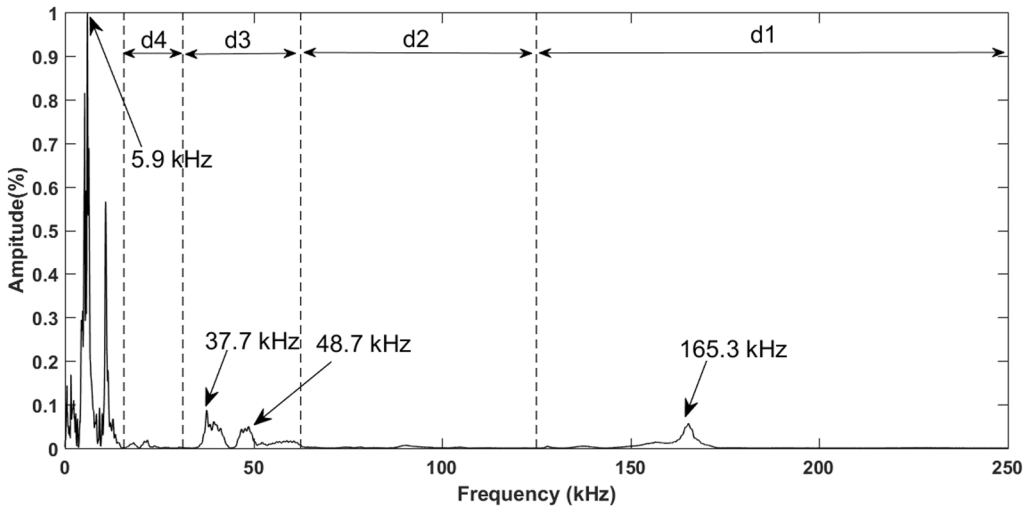

Fig. 4 Layering diagram of wavelet analysis

and viscoelasticity of wood have filtering effect on AE signals in certain frequency bands [16]. So when the stress wave propagates in viscoelastic medium, viscosity is the main factor that causes the attenuation of stress wave at any time and space, so the high-frequency component of the signal attenuates rapidly [34]. Due to high-frequency components decay faster in wood specimens, using correlation analysis can increase the calculation error, so the AE signal in the d3 band was used to calculate the surface wave propagation velocity using correlation. Therefore, the AE signal in the d3 frequency band was used to calculate the surface wave propagation velocity by correlation. Ten independent tests were carried out on four specimens, where v_1 and v_2 denote the propagation velocity at a distance of 150 mm and 300 mm, respectively, and the test results are shown in Table 1.

Table 1 is the surface transverse wave velocity corresponding to different boundary conditions. It can be seen from Table 1 that the velocity of the surface transverse waves varies with the boundary conditions. In the 10 independent tests of T1 specimens without boundary conditions, the average values of v_1 and v_2 are 938 m/s and 949 m/s, respectively. The average values of v_1 and v_2 of sound-absorbing cotton T3 specimens are 938 m/s, the sound-absorbing cotton is loose and porous, which can absorb part of the signal, and the reflection is less than T1, so the speed tends to be stable. However, in T2 and T4 specimens with

Table 1 Propagation velocity of the third layer surface wave under different boundary conditions

Times	T1		T2		T3		T4	
	v_1/m.s^{-1}	v_2/m.s^{-1}	v_1/m.s^{-1}	v_2/m.s^{-1}	v_1/m.s^{-1}	v_2/m.s^{-1}	v_1/m.s^{-1}	v_2/m.s^{-1}
1	938	949	1339	1240	938	938	1119	1042
2	938	949	1339	1240	938	938	1339	1042
3	938	949	1339	1240	938	938	1339	1042
4	938	949	1339	1240	938	938	1364	1042
5	938	949	1339	1240	938	938	1339	1042
6	938	949	1339	1240	938	938	1339	1042
7	938	949	1119	1240	938	938	1339	1042
8	938	949	1339	1240	938	938	1563	1042
9	938	949	1119	1240	938	938	1103	1042
10	938	949	1339	1240	938	938	1103	1042
Average	938	949	1295	1240	938	938	1295	1042

Ten independent tests were carried out on four specimens, where v_1 and v_2 denote the propagation velocity at a distance of 150 mm and 300 mm, respectively, the test results are shown in Table 1.

aluminum plate, the velocity increases obviously. The reason for this change is that although the same reflection phenomenon exists in T2 and T4 specimens, since the propagation speed of AE signal in aluminum plate is greater than that in wood [36], when the AE signal is transmitted to the interface of aluminum plate, the signal is totally reflected, and most of the AE signal is transmitted inside the wood. According to the elastic wave theory, the internal propagation velocity of wood is greater than the surface propagation velocity, which leads to the increase of surface transverse wave velocity when the aluminum plate is added.

Longitudinal velocity of AE signal under different boundary conditions

To explore the effect of boundary conditions on longitudinal wave velocity, the propagation velocity of AE longitudinal wave was calculated by TDOA. Ten independent experiments were carried out on the four specimens, the experimental results are shown in Table 2, where v_{i1} and v_{i2} ($i=1$, 2, 3, 4) represent the propagation velocity at a distance of 150 mm and 300 mm, respectively.

It can be seen from Table 2 that the average propagation velocities of vi_1 and vi_2 are 4688 m/s and 5000 m/s, respectively, indicating that there is no significant change in the propagation velocity of AE signals by changing the boundary conditions. According to the vibration theory of mechanical waves, longitudinal waves can propagate in solid, liquid and gas media. When AE signal propagates from wood to another medium, there is little effect on longitudinal wave.

Energy attenuation law of AE signal under different boundary conditions

To study the energy attenuation law of AE signal under different boundary conditions, the pulse signal with the emission frequency of 150 kHz and the cycle number of 15,000 was generated by the signal generator. In this experiment, the position of the sensor and the AE source was kept unchanged, and the initial energy emitted by the AE source changes as the voltage level was set to 20 V, 15 V, 10 V and 5 V, thus, the energy attenuation can be studied under different boundary conditions and different amplitude conditions. To more intuitively reflect the energy attenuation of each specimen at different amplitudes, Figs. 5 and 6 show the energy attenuation curves of surface and longitudinal waves at different source voltages, respectively. Since the AE energy decays too fast in wood, the real energy is taken as the longitudinal coordinate after logarithm.

The energy attenuation curves of AE surface transverse wave and longitudinal wave under different source voltage levels corresponding to test pieces T1–T4 are shown in (a) to (d) of Figs. 5 and 6, respectively. Although the voltage amplitude is different, the energy attenuation law is basically the same under the same boundary condition. To intuitively express the attenuation trend of energy, the relative distance between each sensor and AE source is taken as the independent variable, and the exponential function is used to numerically fit the energy value of AE signal.

Figures 7 and 8 are the fitting curves of energy attenuation under different voltage levels, which clearly characterize the energy attenuation of different specimens. In the fitting process, the energy measured by the sensor closest to the AE source is regarded as 1, and the energy

Table 2 Propagation velocity of longitudinal waves under different boundary conditions

Times	T1		T2		T3		T4	
	v_{11}/m.s^{-1}	v_{12}/m.s^{-1}	v_{21}/m.s^{-1}	v_{22}/m.s^{-1}	v_{31}/m.s^{-1}	v_{32}/m.s^{-1}	v_{41}/m.s^{-1}	v_{42}/m.s^{-1}
1	4688	5000	4688	5000	4688	5000	4688	5000
2	4688	5000	4688	5000	4688	5000	4688	5000
3	4688	5000	4688	5000	4688	5000	4688	5000
4	4688	5000	4688	5000	4688	5000	4688	5000
5	4688	5000	4688	5000	4688	5000	4688	5000
6	4688	5000	4688	5000	4688	5000	4688	5000
7	4688	5000	4688	5000	4688	5000	4688	5000
8	4688	5000	4688	5000	4688	5000	4688	5000
9	4688	5000	4688	5000	4688	5000	4688	5000
10	4688	5000	4688	5000	4688	5000	4688	5000
Average	4688	5000	4688	5000	4688	5000	4688	5000

Ten independent experiments were carried out on the four specimens, the experimental results are shown in Table 2, where v_{i1} and v_{i2} ($i=1$, 2, 3, 4) represent the propagation velocity at a distance of 150 mm and 300 mm, respectively

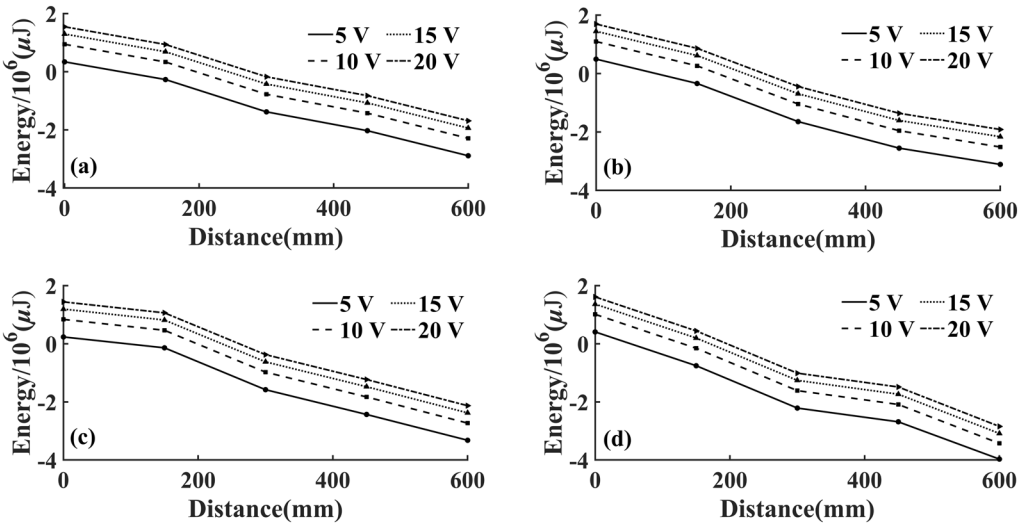

Fig. 5 Energy attenuation curve of AE surface transverse wave

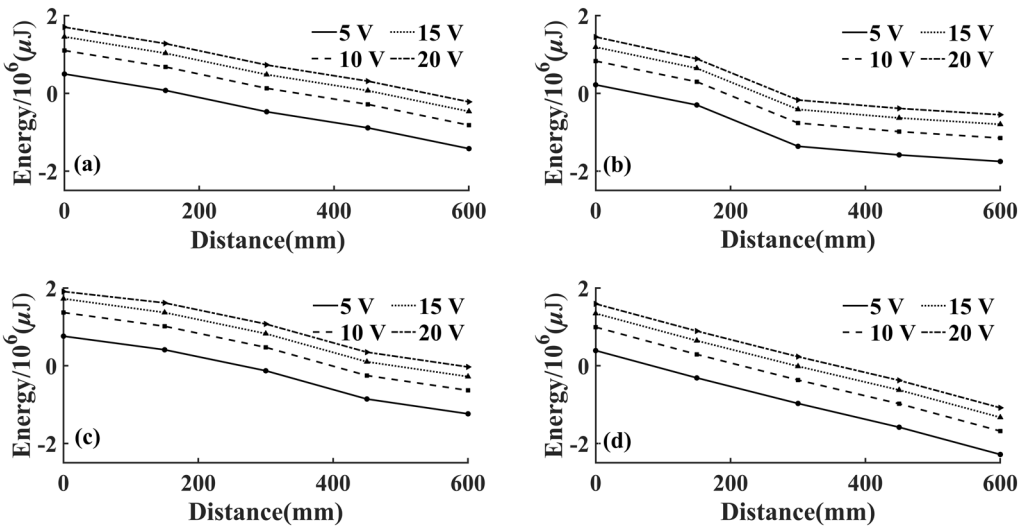

Fig. 6 Energy attenuation curve of AE longitudinal wave

measured by other sensors is normalized to obtain the fitting curve. In the fitting equations shown in Figs. 7 and 8, the coefficient before x is the AE attenuation coefficient under different voltage levels. After calculating the average value, the absolute value is taken, which is called the attenuation rate of this specimen. It is expressed by K. The greater the absolute value of K is, the faster the AE energy attenuation rate is. To show the energy attenuation law of AE signal, the distance from energy attenuation to 50% and 90% and the energy attenuation rate are used to illustrate the energy attenuation.

When characterizing the attenuation law of energy with distance, due to the large attenuation of AE energy, the AE energy is logarithmically processed. There is a significant difference in the order of magnitude between the energy value after logarithm and the distance, and direct fitting is easy to produce a large fitting error. For this reason, the distance is linearly processed in the following:

$$x = \frac{D - \text{mean}(D)}{\text{std}(D)} \tag{4}$$

where D is the actual distance of AE sensor placement, $D \in [0,600\ \text{mm}]$, at this time is the sensor S_1 as the origin;

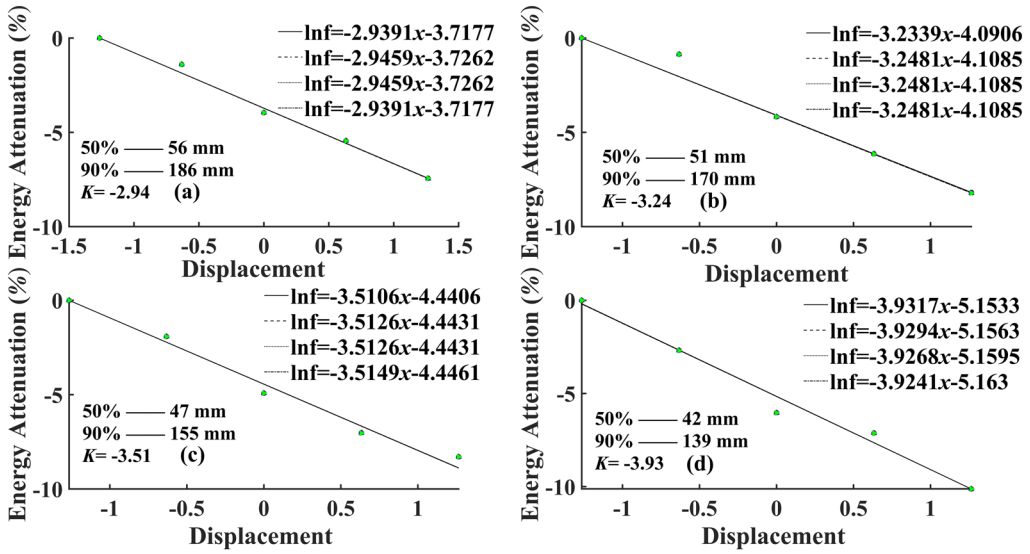

Fig. 7 Fitting curve of AE surface transverse wave energy attenuation

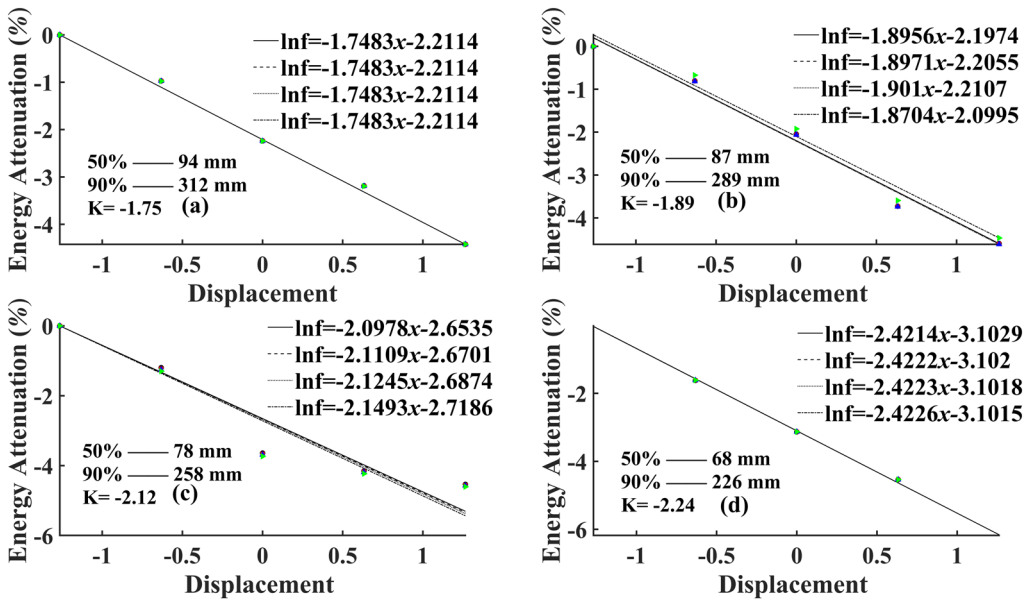

Fig. 8 Fitting curve of AE longitudinal wave energy attenuation

x is the transformed equivalent distance, that is, the horizontal axis coordinates in Figs. 7 and 8; mean(D) is the expectation of D; std(D) is the variance of D. In this paper, the expectation and variance are 300 mm and 237.2 mm, respectively.

The K value in Figs. 7 and 8 is the average slope of the fitting curve of different voltage levels, which represents the attenuation rate of energy. The greater the absolute value of K, the faster the attenuation rate of energy. Comparing Figs. 7 and 8, it can be seen that the $|K|$ of surface transverse waves is greater than that the $|K|$ of longitudinal waves, which means that the surface transverse wave energy decays faster than the longitudinal wave. This is because the longitudinal wave mainly propagates along the internal texture direction of the wood, the propagation resistance is small, so the energy attenuation is slow. But the surface transverse wave mainly propagates along the surface of the wood, which will produce

energy conversion with the surface fluid, and the energy attenuation rate is faster than the longitudinal wave.

It can be seen from Figs. 7 and 8 that in the T1 specimen without any added boundary conditions, the energy attenuation rate $|K|$ of both surface and longitudinal waves is smaller than that of other specimens, and as the boundary conditions are changed, $|K|$ increases gradually, which is mainly due to the different reflection and transmission intensities at different boundaries. Compared with the specimen T2 with aluminum plate, the attenuation rate of T2 was greater than that of T1, which was because the surface transverse wave mainly propagated near the specimen surface, but not completely on the specimen surface, and was greatly affected by the medium in the propagation process [37]. When the AE signal propagates to the boundary condition, the reflection will occur. The propagation velocity of AE signal in aluminum plate is greater than that in wood, so the addition of aluminum plates will make the reflection enhanced and the energy decays fast. Compared with T1 and T3, sound-absorbing cotton is a loose porous medium, adding sound-absorbing cotton will make part of the energy transmission, making the energy decay faster. Compared with the propagation in a single wood specimen T1, the specimen T4 with the addition of aluminum plate and sound-absorbing cotton can result in enhanced reflection and transmission and fast energy decay rate.

To clearly show the attenuation law of energy, the energy attenuation is expressed by the distance of energy attenuation to 50% and 90%, as shown in Fig. 7, the attenuation rate of surface transverse wave in single wood T1 specimen is the slowest, and the attenuation distances to 50% and 90% are 56 mm and 186 mm, respectively. When the boundary conditions were changed, the surface transverse wave attenuation rate of T4 specimen with aluminum plate and sound-absorbing cotton is the fastest, and the attenuation distances to 50% and 90% are 42 mm and 139 mm, respectively. As shown in Fig. 8, the attenuation law of energy during the propagation of longitudinal waves is similar to that of surface transverse waves. The attenuation rate of longitudinal wave in single wood T1 specimen is the slowest, the attenuation distance to 50% and 90% are 94 mm and 312 mm, respectively. When the boundary conditions are changed, the attenuation rate of longitudinal wave in T4 specimen with aluminum plate and sound-absorbing is the fastest, the attenuation distance to 50% and 90% are 68 mm and 226 mm, respectively. According to the attenuation distance in Figs. 7 and 8, the distance from energy attenuation to 50% is shorter than the distance used to increase the attenuation by 40%, indicating that the energy attenuation rate of AE signal is faster in the early stage of propagation, and slower in the late stage. This is mainly because at the initial stage of propagation, AE signals are mainly concentrated in the high frequency band, and the proportion of low-frequency signal components is small, and the high-frequency signal attenuation is obvious in the process of forward propagation.

Conclusions

This paper designed the surface and longitudinal wave extraction experiments for wood based on the theory of elastic and mechanical wave vibrations. The propagation rates of different types of AE signals under different boundary conditions were calculated, and the decay characteristics of AE energy were analyzed.

In the analysis of the velocity, wavelet analysis was used for the surface transverse waves to perform a 4-layer wavelet decomposition of the original AE signal, and it can be found that the main components of the surface transverse waves were concentrated at 37.7 kHz and 165.3 kHz. Since the high frequency signal decays quickly, the third layer detail signal was used to calculate the surface transverse wave velocity. When the boundary conditions were aluminum plate and aluminum plate with sound-absorbing cotton, the surface transverse wave velocity increased in varying degrees compared with the original wood specimen. Since the longitudinal wave and the surface transverse wave propagation medium are different, the longitudinal wave propagation velocity was calculated based on TDOA, and the results of the study showed that the change of boundary conditions had no significant effect on the longitudinal wave velocity. When exploring the AE energy attenuation law, the signal generator was used as the simulated AE source to study the decay of AE energy under different boundary conditions. The change in the initial energy value did not affect the attenuation law of AE energy, and the change in the boundary conditions caused the change in the energy attenuation rate. Under the four different boundary conditions, the surface transverse waves' energy attenuation rates are 2.94, 3.24, 3.15, and 3.93, respectively, and the longitudinal waves' energy attenuation rates are 1.75, 1.89, 2.12, and 2.24, respectively. The energy attenuation of surface transverse wave is more obvious than that of longitudinal wave.

The results of this paper have a great practical significance for AE detection under complex boundary conditions, and provide a basic theoretical basis for how to deal with AE detection data under complex boundary conditions. In the subsequent studies, the propagation and attenuation of AE signals under different boundary conditions can be further quantitatively analyzed.

Abbreviations
AE: Acoustic emission; PLB: Pencil–lead break; TDOA: The time difference of arrival; MC: Moisture content.

Acknowledgements
Not applicable.

Author contributions
ZY conceived the study and designed the methodology; HCL, ZSC, MFL and QGZ conducted the lab work; ZY collected the data, conducted the statistical analysis and led the writing of the manuscript; LM, FSY, DTT and ZDG devised conceptual ideas and provided project support and added substantial edits to the manuscript. All authors contributed critically to the drafts and gave final approval for publication. All the authors read and approved the final manuscript.

Funding
The authors are grateful for the support of the China Natural Science Foundation (NO: 32160345, 31760182) and Department of Education of Yunnan Provincial (NO: 2021J0156, NO: 2021J0158). Startup fund for introducing talents and scientific research of Anhui University of Engineering (NO: 2021YQQ037).

Availability of data and materials
The experimental data used in this study are available on request from the corresponding Author.

Declarations

Competing interests
Conflicts of interest the author declares that he has no conflict of interest.

Author details
[1]School of Machinery and Transportation, Southwest Forestry University, Kunming 650224, Yunnan, China. [2]Key Laboratory of Advanced Perception and Intelligent Control of High-End Equipment of Ministry of Education, Anhui Polytechnic University, Wuhu 241000, Anhui, China. [3]School of Electrical Engineering, Anhui Polytechnic University, Wuhu 241000, Anhui, China.

Received: 30 June 2022 Accepted: 20 November 2022
Published online: 06 December 2022

References

1. Baensch Z, Sanabria SJ, Sause MGR, Pinzer BR, Brunner AJ (2015) Damage evolution in wood: synchrotron radiation micro-computed tomography (SR μ CT) as a complementary tool for interpreting acoustic emission (AE) behavior. Holzforschung 69(8):1015–1025. https://doi.org/10.1515/hf-2014-0152
2. Bobrov AL (2017) Methodical principles of recognition different source types in an acoustic-emission testing of metal objects. J Phys Conf Ser 881(1):012020. https://doi.org/10.1088/1742-6596/881/1/012020
3. Diakhate M, Bastidas-Arteaga E, Pitti RM, Schoefs F (2017) Cluster analysis of acoustic emission activity within wood material: towards a real-time monitoring of crack tip propagation. Eng Fract Mech 180:254–267. https://doi.org/10.1016/j.engfracmech.2017.06.006
4. Kong X, Wang Y, Yang Q, Zhang X, Yang R (2020) Damage identification in fiber reinforced titanium matrix composites using acoustic emission. J Alloy Compd 826:153928. https://doi.org/10.1016/j.jallcom.2020.153928
5. Kawamoto S, Williams RS (2002) Acoustic emission and acousto-ultrasonic techniques for wood and wood-based composites: a review. For Prod. https://doi.org/10.2737/FPL-GTR-134
6. Kim KB, Kang HY, Dong JY, Man YC (2005) Pattern classification of acoustic emission signals during wood drying by principal component analysis and artificial neural network. Key Eng Mater 297–300(Pt3):1962–1967. https://doi.org/10.4028/www.scientific.net/KEM.297-300.1962
7. Nasir V, Cool J, Sassani F (2019) Acoustic emission monitoring of sawing process: artificial intelligence approach for optimal sensory feature selection. Int J Adv Manuf Technol 102(9):4179–4197. https://doi.org/10.1007/s00170-019-03526-3
8. Bucur V, Declercp NF (2006) The anisotropy of biological composites studied with ultrasonic technique. Ultrasonics 44(4):e829–e831
9. Lamy F, Takarli M, Angellier N, Dubois F, Pop O (2015) Acoustic emission technique for fracture analysis in wood materials. Int J Fract 192(1):57–70. https://doi.org/10.1007/s10704-014-9985-x
10. Li XC, Ju S, Luo TF, Li M (2019) Influence of adhesive layer at masson pine glulam on acoustic emission signal propagation characteristics. J Northwest For Univ 34(3):185–190. https://doi.org/10.3969/j.issn.1001-7461.2019.03.29
11. Dong L, Hu Q, Tong X, Liu Y (2020) Velocity-free MS/AE source location method for three-dimensional hole-containing structures. Engineering 6(7):827–834. https://doi.org/10.1016/j.eng.2019.12.016
12. Jeong K, Park KJ (2019) One sensor source localisation of acoustic emissions in thin plates using mode analysis. Insight 61(5):264–270. https://doi.org/10.1784/insi.2019.61.5.264
13. Kuwahara R, Ojima H, Matsuo T, Cho H (2013) Development of acoustic emission waveform simulation technique utilizing a sensor response and finite-difference time-domain method. J Solid Mech Mater Eng 7(2):176–186. https://doi.org/10.1299/jmmp.7.176
14. Markus GR (2011) Investigation of pencil-lead breaks as acoustic emission sources. J Acoust Emiss 29:184–196
15. Yu H, Xiao D, Ma X, Tian H (2014) Near-field beamforming performance analysis for acoustic emission source localization. J Vibroengineering 158(4):127–139. https://doi.org/10.1007/978-1-4939-1239-1_12
16. Wang MH, Deng TT, Fang SY, Li XS, Lai F, Li M (2021) Generation and characteristics of simulated acoustic emission source of wood. J Northeast For Univ 49(6):96–101. https://doi.org/10.13759/j.cnki.dlxb.2021.06.019
17. Wang MH, Deng TT, Ju S, Li XC, Li XS, Li M (2020) Effect of wood surface crack on acoustic emission signal propagation characteristics. J Northeast For Univ 48(10):82–88. https://doi.org/10.13759/j.cnki.dlxb.2020.10.015
18. Shen KN, Zhao HL, Ding XC, Li M (2015) Acoustic emission signal wavelet disjunction in wood damage and fracture process. J Henan Univ Sci Technol 36(3):33–37
19. Fan X, Hu S, Lu J, Wei C (2016) Acoustic emission properties of concrete on dynamic tensile test. Constr Build Mater 114:66–75. https://doi.org/10.1016/j.conbuildmat.2016.03.065
20. Zhao XM, Jiao LL, Zhao J, Zhao D (2017) Acoustic emission attenuation and source location on the bending failure of the rectangular mortise-tenon joint for wood structures. J Beijing For Univ 39(1):107–111. https://doi.org/10.13332/j.1000-1522.20160150
21. Li M, Wang MH, Ding R, Fang SY, Lai F, Luo RH (2021) Study of acoustic emission propagation characteristics and energy attenuation of surface transverse wave and internal longitudinal wave of wood. Wood Sci Technol 55(6):1619–1637. https://doi.org/10.1007/s00226-006-0117-2
22. Ding R, Fang SY, Luo RH, Lai F, Yang ZL, Huang CL, Li M (2022) Propagation characteristics and energy attenuation law of surface shear waves and internal longitudinal waves in Mongolian Scotch Pine sawn timber based on acoustic emission. Chin J Wood Sci Technol 36(1):36–42. https://doi.org/10.12326/j.2096-9694.2021104
23. Ebrahimiana Z, Ahmadi M, Sadri S, Li BQ, Moradian O (2019) Wavelet analysis of acoustic emissions associated with cracking in rocks. Eng Fract Mech 217:106516–106526. https://doi.org/10.1016/j.engfracmech.2019.106516
24. Yu SS, Shen LJ, Li Y, Li M (2017) Acquisition and characteristic analysis of the surface of pinus yunnanensis acoustic emission signal. J Northwest For Univ 32(2):247–251. https://doi.org/10.3969/j.issn.1001-7461.2017.02.42
25. Li Y, Yu SS, Dai L, Luo TF, Li M (2018) Acoustic emission signal source localization on plywood surface with cross-correlation method. J Wood Sci 64(2):78–84. https://doi.org/10.1007/s10086-017-1672-x
26. Liu YF, Yin DM (2005) The depression of the noise in AE from particleboard based on wavelet analysis. J Nanjing For Univ 29(6):91–94. https://doi.org/10.3969/j.issn.1000-2006.2005.06.023
27. Li XS, Deng TT, Wang MH, Luo RH, Li M (2021) Frequency domain identification of acoustic emission signals on surfaceand interior of *Pinus sylvestris* var mongolica based on wavelet analysis. J Northwest For Univ 36(4):209–213. https://doi.org/10.3969/j.issn.1001-7461.2021.04.30
28. Dou CF, Li M, Zhu DG (2021) The detection of hole defects in the simulation of wood borer based on acoustic emission technology. J Cent South

Univ For Technol 41(2):162–170. https://doi.org/10.14067/j.cnki.1673-923x.2021.02.019
29. Jing ZW, Jiang MS, Sui QM, Sai YZ, Lu SZ, Cao YQ, Jia L (2013) Acoustic emission localization technique based on generalized cross-correlation time difference estimation algorithm. Chin J Sens Actuator 26(11):1513–1518. https://doi.org/10.3969/j.issn.1004-1699.2013.11.009
30. Shen KN, Ding XC, Zhao HL, Li M (2015) Acoustic emission signal source localization in wood surface with triangle positioning method. J Northeast For Univ 43(4):77–81. https://doi.org/10.13759/j.cnki.dlxb.20150116.029
31. American National Standard, ASTM-E976 (1993) Standard guide for determining the reproducibility of acoustic emission sensor response
32. Calvet M, Margerin L (2012) Velocity and attenuation of scalar and elastic waves in random media: a spectral function approach. J Acoust Soc Am 131(3):1843–1862. https://doi.org/10.1121/1.3682048
33. Pang HD, Zhang XM, Jiang FX (2004) The spectrum analysis of acoustic emission signal in rock materials. J China Coal Soc 29(5):540–544. https://doi.org/10.1007/BF02911033
34. Teodorovich SB (2003) Technique of measurements of elastic wave attenuation parameters. Russ J Nondestr Test 39(6):427–435. https://doi.org/10.1023/B:RUNT.0000011623.75582.cc
35. Wang GS, Li CH, Hu SL, Feng C, Li SH (2010) A study of time-and spatial-attenuation of stress wave amplitude in rock mass. Rock Soil Mech 31(11):3487–3492. https://doi.org/10.16285/j.rsm.2010.11.023
36. Zhou ZG, Feng ZY, Gao YF, Zhu Z (2008) Application of ultrasonic guided waves to defect inspection of large thin aluminum plate. Acta Aeronaut Astronaut Sin 29(4):1044–1048. https://doi.org/10.3321/j.issn:1000-6893.2008.04.045
37. Qian ZH, Jin F, Hirose S (2011) Dispersion characteristics of transverse surface waves in piezoelectric coupled solid media with hard metal interlayer. Ultrasonics 51(8):853–856. https://doi.org/10.1016/j.ultras.2011.06.005

Publisher's Note